Validation and Refinement of Hyperspectral/Multispectral Atmospheric Compensation Using Shadowband Radiometers

Peter A. Rochford, Prabhat K. Acharya, Steven M. Adler-Golden, Alexander Berk, Lawrence S. Bernstein, Michael W. Matthew, Steven C. Richtsmeier, Stephen Gulick, Jr., and James Slusser

***Abstract*—First-principles atmospheric compensation of Earth-viewing spectral imagery requires atmospheric property information derived from the image itself or measured independently. A field experiment was conducted in May, 2003 at Davis, CA to investigate the consistency of atmospheric properties and surface reflectances derived from simultaneous ground-, aircraft- and satellite-based spectral measurements. The experiment involved the simultaneous collection of HyMap hyperspectral and Landsat-7 multispectral imagery, *in situ* reflectance spectra of calibration surfaces, and sun and sky radiances from ultraviolet and visible multifilter rotating shadowband radiometers (MFRSRs). The data were analyzed using several different radiation transport and atmospheric compensation algorithms. Reasonable self-consistency was found between aerosol property retrievals from the radiometers and from dark pixels of the imagery, and, when using the most accurate algorithm, there was excellent agreement between the retrieved surface spectra and the ground truth measurements.**

***Index Terms*—Atmospheric, compensation, correction, HyMap, hyperspectral, radiometer, shadowband.**

I. Introduction

THE spectral coverage and resolution afforded by visible/short-wave infrared hyperspectral and multispectral imaging (HSI and MSI) systems provide a wealth of information for remote sensing of the Earth surface. However, optimum use of these data requires processing with an atmospheric "correction" or "compensation" step, which removes the effects of light scattering and absorption by aerosols, haze, and gases, and retrieves surface reflectance spectra. Because highly accurate reflectances are needed for many applications, evaluation of atmospheric compensation accuracy and development of improved algorithms are very active areas of research.

First-principles methods of atmospheric compensation, used when "ground truth" reflectance spectra are unavailable, require knowledge of atmospheric properties, including aerosol optical depth (or visibility) and column water content. In favorable situations, many of these properties may be estimated from the image itself; otherwise, they must be obtained from independent measurements. One potential source of the latter data is ground-based spectral radiometers. These include pointing instruments such as the Cimel Sunphotometer, which spatially resolves the sky radiance, and whole-sky instruments such as the Yankee Environmental Systems (YES) multifilter rotating shadowband radiometers (MFRSRs) [1], which measure total direct and diffuse fluxes. These instruments can provide information on column concentrations of water vapor, ozone, and other gases, as well as information on the aerosol optical depth, single-scattering albedo and (from the Cimel) scattering phase function at various wavelengths.

Ground-based radiometer data both overlap and complement information obtainable from spectral imagery of the ground. Many of the parameters that can be retrieved from these two types of data are nominally the same, such as column water vapor and aerosol optical depth. However, the derived parameter values may differ, due to differences in wavelength coverage, measurement geometry, retrieval assumptions, or location of the sensors. For example, aerosol optical depth (AOD) is often inferred from imagery using dark pixels with assumptions about the surface reflectance and the aerosol single-scattering albedo (SSA) and scattering phase function. In contrast, AOD is derived from radiometer data via the inferred solar absorption, which is independent of these assumptions, but is subject however to uncertainty in the instrument's calibration. Because of these differences, the best way to incorporate radiometer data into the atmospheric compensation process is not obvious.

Although the basic physical phenomena involved in both the remote and ground-based measurements appear to be well understood, some anomalies have been noted. Schoemaker and deLeeuw [2] compared 550-nm AOD values retrieved from the Along Track Scanning Radiometer (ATSR)-2 sensor on the European Remote Sensing (ERS)-2 satellite with results from two Aerosol Robotic Network (AERONET) radiometer sites in Europe. While the overall AOD agreement was good, the ATSR-2 values averaged several hundredths higher than the radiometer retrievals. Other studies (e.g., Ricchiazzi and Gautier [3], Halthore and Schwartz [4]) have found a different but perhaps related problem, in which shadowband radiometer diffuse-to-direct flux ratios were lower than expected at low AOD. This was interpreted in terms of anomalous atmospheric absorption, or, equivalently, lower-than-expected values of the

Manuscript received May 24, 2005; revised August 24, 2005. This work was supported in part by the National Aeronautics and Space Administration under SBIR Contract NAS13 02056. MFRSR data analysis at Colorado State University is supported by the U.S. Department of Agriculture under the UV-B Monitoring and Research Program.

P. A. Rochford, P. K. Acharya, S. M. Adler-Golden, A. Berk, L. S. Bernstein, M. W. Matthew, and S. C. Richtsmeier are with Spectral Sciences, Inc., Burlington, MA 01803 USA (e-mail: sag@spectral.com).

S. Gulick, Jr. is with ITT Space Systems, Rochester, NY 14653-7208 USA.

J. Slusser is with Natural Resource Ecology Laboratory, Colorado State University, Fort Collins, CO 80523 USA.

Digital Object Identifier 10.1109/TGRS.2005.857901

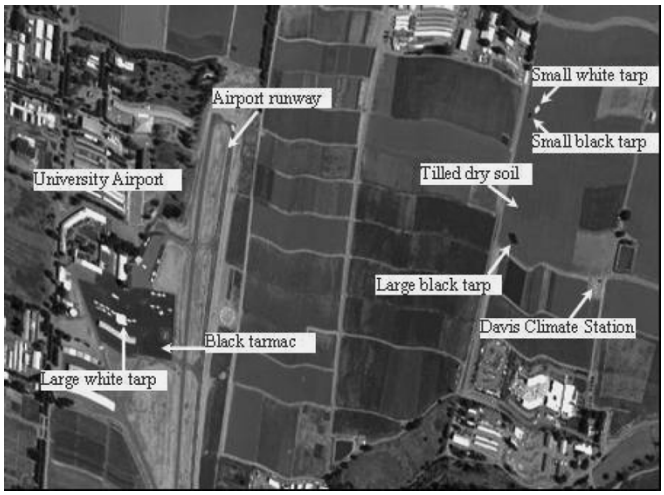

Fig. 1. HyMap image showing the locations of calibration surfaces at UC Davis campus and University Airport during the May 31, 2003 field experiment. The radiometers were at the Davis Climate Station.

aerosol SSA. Such uncertainties are relevant to atmospheric compensation, as they translate into retrieved surface reflectance uncertainties in the visible region of order 0.01–0.02 for a nadir-viewing sensor, and larger uncertainties for off-nadir viewing.

In this paper, the use of MFRSR data for spectral image compensation is investigated using data from a field experiment at Davis, CA in which atmospheric and surface properties were retrieved from a combination of remote and ground-based instruments. Sun and sky radiation measurements were made by visible (VIS) and ultraviolet (UV) MFRSRs. Ground truth surface reflectances were measured using a field-calibrated portable spectrometer. In addition, simultaneous imagery was collected from the Hyperspectral Mapper (HyMap) airborne sensor and the Landsat-7 satellite. Two industry-standard codes were used to atmospherically correct the imagery: Fast Line-of-sight Atmospheric Analysis of Spectral Hypercubes (FLAASH) [5], [6] and Atmospheric Corection Now (ACORN) [7]. These codes, which utilize Moderate resolution Transmission (MODTRAN) [8] radiation transport modeling, provide the options of using independent aerosol information or automatically estimating the average visibility from the image itself. A new version of FLAASH was developed for this study that allows adjustment of the SSA and the wavelength dependence of the aerosol model. Two different codes were used to analyze the MFRSR data. The results of this study include assessment of the accuracy and self-consistency of the atmospheric compensations from FLAASH and ACORN and the atmospheric parameter retrievals from the MFRSRs.

II. Data Description

The field experiment took place on May 31, 2003 at Davis, CA near the U. S. Department of Agriculture (USDA) UV-B Monitoring and Research Program site, the University of California campus, and the University Airport (see Fig. 1). The field experiment involved the simultaneous collection of imagery from the HyMap aircraft sensor (Hyvista Corp., Sydney, Australia), the Landsat-7 satellite, *in situ* reflectance spectra of calibration surfaces, and sun and sky radiation measurements from two YES shadowband radiometers located at the USDA research station.

TABLE I
Collected Remote Imagery

Flight	HyMap 1	HyMap 2	HyMap 3	Landsat-7
Greenwich Mean Time (GMT)	16:19	16:50	20:28	18:36
Local Daylight Saving Time	9:19 AM	9:50 AM	1:28 PM	11:36 AM
Sensor Altitude (km)	1.17	2.46	1.19	705
Average Pixel Size (m)	2.4	5.5	2.4	25

The HyMap aircraft collected three hyperspectral data strips along an east-west flight path between the Davis airport and Sacramento, approximately 30 km to the east. The first two strips were acquired back-to-back at approximately 9:19 A.M. and 9:50 A.M., and the third strip was acquired at approximately 1:28 P.M. For ease of reference we label these strips as HyMap 1 through HyMap 3. Characteristics of the flights and the radiance imagery collected are listed in Table I. The sensor covers the ~450–2500-nm wavelength range in 126 spectral channels with an average 16-nm full width at half-maximum (FWHM). Hyvista Corp. provided the data as both calibrated spectral radiance and as spectral reflectance, where the latter was obtained from Hyvista's processing with ACORN.

The Landsat-7 satellite acquired image no. LE7044033000315150 over the Davis-Sacramento area at approximately 11:36 A.M., only 3 h prior to failure of its scan line corrector at around 21:45 GMT. The data cover the visible, shortwave infrared, and near-infrared (VIS-SWIR-NIR) spectral regions in six bands centered at approximately 480, 560, 660, 830, 1650, and 2200 nm.

An examination of the brightest pixels of the HyMap data revealed that the sensor response was saturated in some visible channels in the second and third data strips. This saturation produces small dips around 500–600 nm in the brightest spectra from the second strip, and larger and more extensive dips in the spectra from the third strip. Although this effect complicates the data analysis, it should not have affected the retrieval of atmospheric parameters from other spectral regions and from dark pixels, or the atmospheric compensation of less bright pixels.

Four calibration tarps varying in approximately square size from 10–20 m were placed around the USDA site and the airport as indicated in Fig. 1. Two of these were tarps consisting of white Tyvek polyethylene fabric [9], and the others were black tarps composed of several layers of a black geotextile. The large white tarp was placed on the tarmac of the UC Davis airport, while the small piece and the black tarps were placed in a recently tilled dirt field near the UC Davis airport. Spectral measurements of the tarps over the 0.4–2.5-μm wavelength range were taken using a hand-held Analytical Spectral Devices (ASD) FieldSpec Pro spectroradiometer. These measurements were normalized to a Spectralon (unit Lambertian reflectance) surface to generate absolute reflectance spectra. Reflectance measurements were similarly made for a few large, spatially uniform surfaces that include the black tarmac at the airport and dry soil at the recently tilled agricultural field. In addition,

several measurements of the direct and diffuse sky spectral irradiance were made with the Remote Cosine Collector (RCR) foreoptic on the spectroradiometer.

Two YES Multifilter Rotating Shadowband Radiometers (MFRSRs), a visible instrument and a UV instrument, were in continuous operation at the UC Davis Climate Station during the field experiment. The visible data are available through the USDA Shadowband Network on the Internet at http://uvb.nrel.colostate.edu. The seven-channel visible MFRSR (VIS-MFRSR) provided total horizontal, direct normal and diffuse radiation at filtered wavelengths of 415, 500, 610, 665, 862, and 940 nm at a nominal 10-nm FWHM bandwidth. The seventh channel measured the unfiltered broadband spectrum. The seven-channel UV-MFRSR provided corresponding radiance measurements at 300, 305.5, 311.4, 317.6, 325.4, 332.4, and 368 nm at a nominal 2-nm bandwidth. The VIS-MFRSR and UV-MFRSR data are recorded every 15 and 20 s, respectively, and provided as 3-min averages in flux units (watts per square meter per nanometer) by the onboard computer. In addition, all stations in the USDA Shadowband Network are instrumented with meteorological sensors that provide ancillary data on atmospheric conditions. The humidity and temperature can be used to define the surface values in the atmospheric model profiles used by the analysis algorithm. However, the atmospheric retrieval algorithm is not very sensitive to these values.

III. Radiometer Data Analysis

A. VIS Data

The VIS-MFRSR data analysis was performed with an algorithm dubbed MISAR (MODTRAN Inferred Shadowband radiometer Atmospheric Retrieval), which is briefly outlined here. Since the instruments at Davis had not been calibrated in many years, Langley methods were used to convert the relative (voltage) units of measurement to absolute flux units. That is, the relative top-of-the-atmosphere (TOA) direct flux is inferred from the data by assuming Beer's law, and the result is compared with the predicted absolute flux. The latter is calculated from the TOA solar irradiance function corrected for the Earth-to-Sun distance and convolved with the bandpass filter response functions. The solar function is from the corrected Kurucz [10] database, which is the standard in MODTRAN. The ratios of the predicted to inferred fluxes provide calibration factors for each spectral band, which are applied to both the direct and diffuse measurements. Averaging the A.M. and P.M. calibration factors minimizes the effect of a systematic trend in the atmosphere over the course of the day. All of the MFRSR channels except the 940-nm water-vapor channel (band 6) obey Beer's law and are amenable to this analysis. A method for utilizing uncalibrated 940-nm data is described by Michalsky [11]. Since the 940-nm water vapor channel was not properly calibrated, our analysis used the water vapor amount derived from the FLAASH atmospheric compensation of the HyMap data.

To improve the signal-to-noise, cloud-free data in 40-min time periods bracketing the remote sensor overflights were selected and averaged, resulting in representative flux measurements for each band and overflight. The results were analyzed with the iterative MISAR algorithm to yield ozone and aerosol model parameters. The average surface albedo, an input to which the results are only slightly sensitive, was estimated from the atmospherically corrected HyMap imagery as [0.04, 0.06, 0.10, 0.10, 0.25, and 0.26] for the six narrow-band VIS-MFRSR channels at 415, 500, 610, 665, 862, and 940 nm, respectively. The starting model atmosphere was specified as the standard MODTRAN midlatitude summer atmosphere with the rural aerosol model and a spring-summer profile for the tropospheric and stratospheric aerosols. The MISAR procedure rescales the atmospheric water vapor and ozone amounts and modifies the aerosol properties, as described below. Since the sensitivity of the results to temperature is very slight, the use of a standard atmosphere model instead of one based on the surface meteorology makes little difference in the retrievals, and it ensures consistency with the FLAASH atmospheric compensation.

We have chosen to represent the modified aerosol model by the formula

$$\tau_{\rm aer}(\lambda) = \tau^R_{\rm aer}(\lambda)\left(\frac{\lambda o}{\lambda}\right)^{\Delta N} \tag{1}$$

where $\tau^R_{aer}(\lambda)$ is the optical depth of the reference aerosol and ΔN is an adjustable parameter suggested by the Angstrom law (power-law dependence on wavelength) [12]. This model, which is incorporated in our most recent MODTRAN version 4.9, has several attractive properties: 1) it yields the general Angstrom-law model for an Angstrom-law reference aerosol; 2) it reduces to the reference aerosol in the limit of $\Delta N = 0$; and 3) it extrapolates well into the infrared, making it useful with VIS-SWIR-NIR imagery.

A complete specification of the aerosol includes definition of its scattering properties via the SSA and phase function. The MISAR algorithm defines the SSA with respect to the reference MODTRAN aerosol model via a scaling factor that multiplies the spectral co-albedo (1-SSA). The phase function is likewise taken from the reference aerosol. The phase functions for all of the standard MODTRAN aerosols are very similar. While their co-albedos are different, introduction of the co-albedo scaling factor as a variable reduces the sensitivity of the results to the choice of reference aerosol model.

The retrieval algorithm uses a series of MODTRAN transmittance calculations to iteratively fit the direct solar fluxes with the aerosol model in (1) and a scale factor that multiplies the initial-guess ozone concentration. In this fit, channel 6 is omitted since it has strong water absorption, and the poorest fitting channel of the remaining five is also omitted. If channel 6 is calibrated, a scale factor for the water vapor profile is retrieved, and the previous step repeated with the scaled water vapor profile. Finally, the sum of the diffuse fluxes in channels 1–5 is iteratively fit to derive the co-albedo scale factor. The outputs include values for the visibility, AOD at each wavelength, ΔN, co-albedo scale factor, and column ozone scale factor and amount. The total AOD is the sum of AODs from boundary layer and upper atmospheric aerosols; the latter contributions are very small unless a

TABLE II
VIS-MFRSR-RETRIEVED ATMOSPHERIC PROPERTIES FOR IMAGERY. SCALE FACTORS ARE RELATIVE TO MID-LATITUDE SUMMER ATMOSPHERE, RURAL AEROSOL. VALUES IN PARENTHESES ARE FROM THE USDA CALIBRATION. FOR REFERENCE, THE UV-MFRSR AOD IS LISTED

Quantity	HyMap 1	HyMap 2	HyMap 3	Landsat-7
Solar zenith angle (°)	49.7	42.7	16.9	25.3
ΔN	0.41 (0.02)	0.50 (0.07)	0.64 (0.02)	0.50 (0.04)
Aerosol Co-albedo Scale Factor	2.6 (2.1)	1.7 (0.7)	0.0 (0.0)	0.0 (0.0)
550 nm SSA	0.91	0.97	1.00	1.00
550 nm AOD	0.152 (0.141)	0.134 (0.128)	0.093 (0.084)	0.122 (0.114)
Visibility (km)	53 (56)	61 (65)	96 (110)	69 (75)
Ozone Column Scale Factor	1.21 (0.63)	1.27 (0.64)	1.20 (0.49)	1.26 (0.53)
368 nm AOD (UV-MFRSR)	0.21	0.22	0.21	0.25

volcanic profile is specified. Visibility, or meteorological visible range, is related to the boundary layer 550-nm AOD via

$$\text{visibility (km)} = \frac{\ln(50)}{(E550 + 0.011\,59\ \text{km}^{-1})}. \qquad (2)$$

Here E550 is the surface horizontal extinction per kilometer at 550 nm, which is equal to the boundary layer AOD divided by the effective layer thickness, a quantity that depends on MODTRAN's vertical aerosol profile model. The effective layer thickness is AOD- and elevation-dependent, but is typically around 2 km.

The VIS-MFRSR quantities retrieved for the times of the HyMap and Landsat-7 images are presented in Table II. Because the AODs are low, the accuracy of the results is limited by their high sensitivity to the radiometric calibration. Results from two different calibration analyses are presented to indicate the rough size of the error bars. The initial calibration was performed using a variant of the Langley plot method, in which $ln(v)/M$ is plotted versus $1/M$ (v is voltage, and M is air mass); the TOA voltage is given by the slope of the plot. This method may be marginally more accurate than the standard Langley method of plotting $ln(v)$ versus M, as it spreads the data more evenly along the x axis and weights them uniformly in extinction coefficient (J. B. Kerr, private communication; S. Adler-Golden, unpublished work). The second set of results is from the USDA/Colorado State Langley-calibrated data, which became available late in the program.

As seen in Table II, most of the retrieved quantities are reasonably well determined. The key exception is the ozone amount, its large uncertainty being related to the weakness of its visible light absorption. The most accurate ozone measurement, from the UV data, indicates a daily average of 330 Dobson units (scale factor of 1.00).

B. UV Data

The UV-MFRSR data were processed using the algorithm of Petters [13], which is functionally similar to MISAR. Since in the UV there are no significant molecular features with fine spectral lines, this algorithm does not require a spectral band model such as MODTRAN for radiation transport modeling. The Langley method was used to establish the absolute radiometric calibration. The calibration accuracy was optimized by combining ∼20 days of measurements. The May 31, 2003 results, which were reported as a function of time, include 368-nm AOD and SSA and an Angstrom exponent describing the aerosol wavelength dependence.

The retrieved 368-nm AODs corresponding to the time windows used for the VIS-MFRSR data analysis are listed in Table II. The SSA has an essentially constant value of 0.75, with an estimated error bar of 0.10. The Angstrom coefficient is 1.3 ± 0.1. Using this value to extrapolate the AOD to 550 nm yields AOD values that differ from the VIS-MFRSR values by up to 0.03; however, the averages of the two set of values agree to within 0.01. Considering the uncertainties in MFRSR calibrations and the differences in the UV and VIS data processing methods, this level of agreement seems reasonable.

IV. IMAGERY ANALYSIS

A. Atmospheric Compensation Algorithms

The HyMap data were supplied by Hyvista Corp. in both atmospherically corrected (reflectance) and uncorrected (spectral radiance) forms; the former were calculated using the ACORN code (available from ImSpec LLC). The Landsat-7 data from NASA, in calibrated radiance units, were atmospherically corrected using a modified β version of ENVI FLAASH 4.1 (available from Research Systems, Inc.), called FLAASH-MISAR. The FLAASH code [5], [6], developed by Spectral Sciences, Inc. and the Air Force Research Laboratory (AFRL) with additional support from other U.S. Government agencies, was designed primarily for imagery over land. The new FLAASH-MISAR version features an interface that allows some or all of the atmospheric parameters retrieved from MFRSR data (ΔN, co-albedo scale factor, visibility, water, and ozone scale factors) to be used for atmospheric compensation.

The FLAASH and ACORN algorithms differ in several ways. ACORN retrieves a measure of surface liquid water content while FLAASH does not. FLAASH uses a more recent version of MODTRAN with a newer spectral database. FLAASH uses a reflectance ratio-based method for visibility retrieval, while ACORN uses a proprietary method based on spectral shape matching between 400–1000 nm. FLAASH performs the MODTRAN calculations on-the-fly, supporting off-nadir geometries and all MODTRAN aerosol types, while ACORN interpolates from a set of precalculated lookup tables. In addition, FLAASH provides compensation for the adjacency effect (a blending of nearby surface spectra due to atmospheric scattering) and automated wavelength calibration. The results from FLAASH and ACORN tend to be similar in dry, clear atmospheres [14], but significant differences can occur under moist and hazy conditions [6].

B. FLAASH Procedure

The FLAASH atmospheric compensation method is outlined in several papers [5], [6]. Of particular interest here is the retrieval of aerosol information. Over land it is usually practical to retrieve only the average aerosol amount, as defined by optical depth or visibility. FLAASH retrieves visibility by assuming a

characteristic reflectance ratio for dark pixels in two wavelength bandpasses. A description of the method, which has evolved somewhat and which has not been fully presented elsewhere, is given here. The method provides a solution to the equation for at-sensor radiance

$$L^* = \frac{A\rho}{(1-\rho_e S)} + \frac{B\rho_e}{(1-\rho_e S)} + L_a^* \tag{3}$$

where ρ is the pixel surface reflectance, ρ_e is an average surface reflectance for the pixel and a surrounding region (defined by spatially convolving ρ with an adjacency point spread function), S is the spherical albedo of the atmosphere, L_a^* is the radiance backscattered by the atmosphere, and A and B are coefficients that depend on atmospheric and geometric conditions.

First, radiance images in each of the two bandpasses, which may be single wavelength channels or averages of channels, are gathered from both the original data cube and from L_e^*, the radiance convolved with the adjacency point spread function. MODTRAN calculations are then carried out to determine A, B, S, and L_a^*, for a series of trial visibility values. For the highest trial visibility, the results are used to perform an initial image compensation for the bandpass used to define the dark pixels; ideally, this is the longer-wavelength bandpass, which is less sensitive to the assumed visibility value. A reflectance upper limit value is then applied to the results to select the dark pixels. For the selected dark pixels, reflectance solutions are calculated for both bandpasses and each trial visibility. Then a reflectance error for the shorter-wavelength bandpass (the difference between the calculated reflectance and the calculated longer-wavelength reflectance times the assumed ratio) is tabulated for each pixel. A visibility estimate may be obtained by interpolating the reflectance error to find the value that yields zero error. To efficiently calculate a scene-average visibility, the reflectance errors for all the dark pixels are averaged, and the interpolation is performed on the result.

The above ratio-based method is applied to land imagery in FLAASH following the work of Kaufman *et al.* [15], which is based on the empirical observation of a characteristic reflectance ratio for dark land surfaces for wavelengths of ∼660 and ∼2200 nm. They found this ratio to be 0.5 from images over the mid-Atlantic United States, with a 10% to 20% reduction in drier regions. In FLAASH the default ratio is 0.45, and the dark pixels are defined as having a 2200-nm reflectance upper limit of 0.1. In a refinement of this procedure, developed at the Spectral Information Technical Applications Center (SITAC), water and shadow pixels are identified and excluded from the dark pixel set. The identification is based on a ratio of 400–450-nm radiance to 750–865-nm radiance, where values greater than 1 indicate water or shadow (D. Miller and S. Sarlin, private communication).

The ratio-based retrieval may be implemented with a different set of bandpasses, and without the water/shadow exclusion, in order to derive visibility from reasonably deep and clear water pixels. For example, Adler-Golden *et al.* [12] used bandpasses at ∼900 and ∼2200 nm with a reflectance ratio of 1.0 and a 2200-nm reflectance upper limit of 0.015 to retrieve visibility from littoral zone imagery. When we applied this method to the Davis imagery, it identified many suitable small water bodies such as ponds, swimming pools, and a stream. However, it also found flooded fields, presumably used for rice cultivation, where the water is very shallow, perhaps a few inches deep. These field pixels are more reflective than deep water in the shorter wavelength bandpass, and therefore yield anomalous visibility results. A solution to this problem is to set the reflectance upper limit with the shorter wavelength bandpass to weed out the shallow water pixels; we have found that a value of around 0.03 typically works well. A disadvantage of this procedure is that since the shorter wavelength is much more sensitive to the assumed visibility, many valid dark pixels are excluded when the true visibility is much lower than the high-visibility initial trial used for the pixel selection. This drawback could be addressed by making the pixel selection method visibility dependent.

In the current work we generally used a shortcut for retrieving visibility from the HyMap data, which was to first resample the data to Landsat-7 spectral bands. Bands 3 and 6 were used with the land pixel method, and bands 4 and 6 were used with the water pixel method. Since the visibility retrieval algorithm is based on broad bandpasses, there should be little if any reduction in accuracy due to the resampling. In addition to saving computation time, the resampling allowed the HyMap and Landsat-7 data to be processed in exactly the same manner, facilitating comparison of the results. A comparison of visibility retrievals from the resampled HyMap image 1 and from the original hyperspectral data found very close agreement (24 versus 25 km, respectively) using the land method with the rural aerosol model.

The FLAASH visibility retrieval and atmospheric compensation can be sensitive to the method selected for the MODTRAN multiple scattering calculations. The Isaacs [16] two-stream method, the discrete-ordinate radiative transfer (DISORT) method [17] with eight streams, and a method called "DISORT scaling" [8] which uses a small number of DISORT calculations to scale two-stream multiple scattering calculations, all gave very similar results (within 1 km in visibility) with the present data. The DISORT scaling method, which has the best combination of speed and accuracy, was used in the work reported here.

Because the aerosol retrieval bandpasses are in atmospheric window regions, the results are insensitive to the assumed atmospheric water vapor content. The Landsat-7 data analysis assumed the Midlatitude Summer atmospheric model water vapor. The HyMap data analysis followed the usual FLAASH procedure for hyperspectral data, in which a initial water vapor retrieval is performed, the average result is used for visibility retrieval, and the water vapor is refined using the retrieved visibility.

C. Visibility Retrievals

As reported by Hyvista, the visibilities retrieved by ACORN for the HyMap images 1, 2, and 3 were, respectively, 140, 250, and 250 km. These values are much higher than the MFRSR results of ∼50–100 km, and lead to inaccuracy in the retrieved reflectance spectra, as shown below.

To test for parameter sensitivities, visibilities were retrieved by FLAASH for several different trial atmosphere models using

TABLE III
FLAASH-MISAR VISIBILITY RETRIEVALS FROM LANDSAT-7 IMAGE OF DAVIS (LAND PIXEL METHOD)

ΔN	CSF	Ozone SF	Visibility (km)
0.	1.	1.	77
0.	6.	1.	33
0.	3.5	1.	47
0.4	3.5	1.	54
0.4	3.5	1.24	50

TABLE IV
FLAASH-MISAR VISIBILITY RETRIEVALS FROM HYMAP IMAGE 2 (OZONE SF = 1.24)

ΔN	CSF	Method (Land/Water)	Visibility (km)
0.4	3.5	Land	23
0.4	1.	Land	29
0.	1.	Land	30
0.4	3.5	Water	27
0.4	1.	Water	35
0.	1.	Water	38

both the land-based and water-based algorithms. The co-albedo scale factor (henceforth denoted CSF) was varied between 1 and 6 to cover nearly the full range of SSA values retrieved by the two radiometers. Two ΔN values, $\Delta N = 0$ and 0.4, were taken to cover the values spanned by the "base" aerosol model and the VIS-MFRSR results. In addition, sensitivity to the ozone was examined by using two different scale factors, 1.0 and 1.24.

For the higher altitude HyMap data (image 2) and the Landsat-7 data, the FLAASH visibilities were in the general range of 30–80 km using different retrieval methods and aerosol models. For such clear conditions, differences among the reflectance retrievals are small. For the lower altitude HyMap data (images 1 and 3), lower-than-expected visibilities were obtained, in the neighborhood of 25 km. We surmise that these low visibilities are the result of the aerosol being closer to the ground than assumed by MODTRAN, so that a higher-than-expected amount of aerosol backscattering occurs between the ground and the sensor for a given aerosol column. This effect, which may be due to overestimation of the boundary layer thickness and/or the upper atmospheric AOD, should have a minimal impact on the reflectances for dark pixels, but should cause some overcompensation of very bright pixels such as the white tarp.

Example results using the land pixel method are shown in Table III for a 400×400 pixel portion of the Landsat-7 image covering the Davis area. The retrieved visibilities illustrate the sensitivity to the aerosol parameters and the ozone scale factor. There is relatively little dependence on ΔN and the ozone scale factor, but a significant dependence on the CSF. The high CSF value of 6 $(\text{SSA} \sim 0.74)$ indicated by the UV-MFRSR gives a visibility that is clearly too low. The most reasonable visibility is obtained with $\text{CSF} = 1.0\,(\text{SSA} \sim 0.96)$, a value consistent with the VIS-MFRSR data to within error limits. Since the wavelengths used for aerosol retrieval, 0.66 and 2.2 μm, are within or beyond the visible region, this result confirms the MFRSR trend of increasing SSA with longer wavelengths.

Further study of the Landsat-7 scene suggests some geographic variation in the aerosol. For example, when a much larger portion of the image (1500×3000 pixels) that includes Sacramento was analyzed, the retrieved visibility in the first case of Table III dropped from 77 to 51 km. When the water pixel algorithm was used, most of the water pixels were from a lake northeast of Sacramento, where the retrieved visibility was relatively low, around 30 km. When the lake pixels were masked, a more typical visibility of around 50 km was obtained.

Results are shown in Table IV for the HyMap image 2. Since this high-spatial-resolution image contains some whole pixels of small water bodies (a stream, pond, and swimming pools) we include results from the water pixel method. Here the visibilities tend to be lower than the MFRSR and Landsat-7 results, particularly with the land pixel method. This difference is in the same direction as for the low-altitude images 1 and 3 but is smaller. The discrepancy between the typical FLAASH-derived visibility of ~30 km and the lower limit estimate from the VIS-MFRSR of ~50 km amounts to a 550-nm AOD difference of 0.09. It should be noted that since in the water pixel method the aerosol-sensitive wavelength of ~ 0.83 μm is at the long-wavelength end of the MFRSR measurement range, the trend of increasing SSA (decreasing CSF) with wavelength would make the highest CSF value most appropriate for visibility determination, thus minimizing the discrepancy with the MFRSR results.

To check if the discrepancy between the Landsat-7 and HyMap image 2 visibility retrievals may be related to the differences in spatial resolution, we reanalyzed HyMap image 2 after resampling to the Landsat-7 pixel size. The result was a 5-km decrease in visibility, which is smaller than the difference with Landsat-7 and in the opposite direction.

We conclude the bulk of the visibility discrepancy is not caused by the spectral resolution difference per se, but is likely the same as in HyMap images 1 and 3—namely, a combination of low sensor altitude and inaccurate modeling of the aerosol vertical profile by MODTRAN. This explanation is supported by comparing the AOD from the ground to the sensor with the total AOD to the TOA. With $\text{CSF} = 1$, an ozone scale factor of 1, and the water pixel method, the visibility retrieved from HyMap image 2 is 40 km, for which MODTRAN's standard aerosol vertical profile gives a total AOD at 550 nm of 0.195. However, the FLAASH retrieval is sensitive not to the total AOD but to the AOD from the sensor, which is 0.125 with this profile. If instead of following this profile the aerosol were negligible above the sensor, this AOD would represent the total AOD measured by the MFRSRs. The result would be an MFRSR-retrieved visibility of 67 km, consistent with the data.

D. FLAASH Column Water Vapor Retrievals

FLAASH retrieved atmospheric column water amounts of around 2.3 cm from HyMap image 1 and 2.0 cm from image 2. Since the shape of the vertical profile is not known, the difference between these values may be due to the difference in viewing geometries. We are unaware of independent ground truth information on the water vapor profile (such as radiosonde data) for the location and time of the experiment. However, the FLAASH-retrieved values are close to an estimate based on

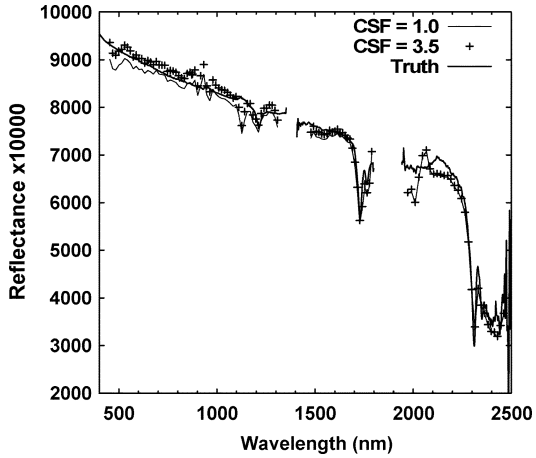

Fig. 2. FLAASH-MISAR retrievals from HyMap image 1 for the large white tarp. Visibility is 50 km, $\Delta N = 0.4$, and ozone SF $= 1.24$.

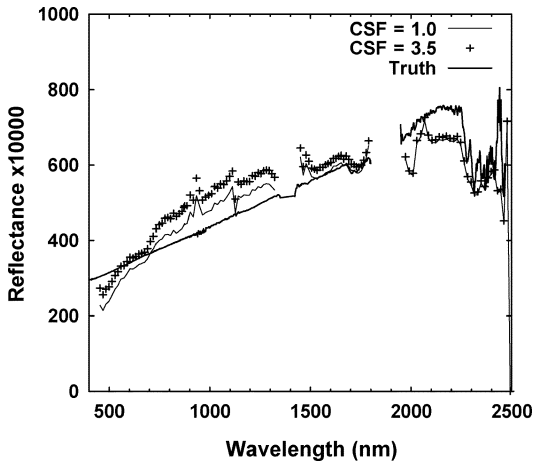

Fig. 3. FLAASH-MISAR retrievals from HyMap image 2 for the large black tarp. Visibility is 50 km, $\Delta N = 0.4$, and ozone SF $= 1.24$.

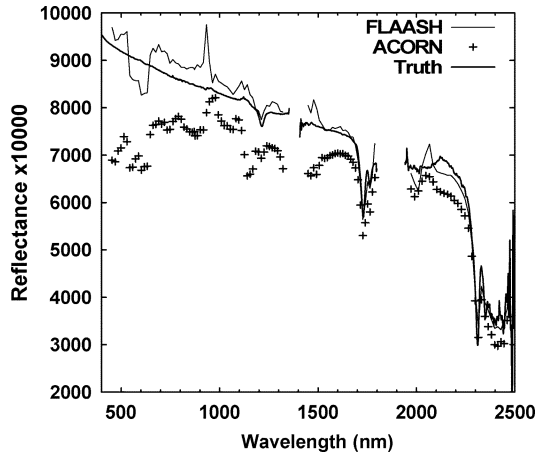

Fig. 4. Default retrievals from FLAASH and ACORN from HyMap image 2 for the large white tarp. The bite-outs below 625 nm are due to saturation of the sensor.

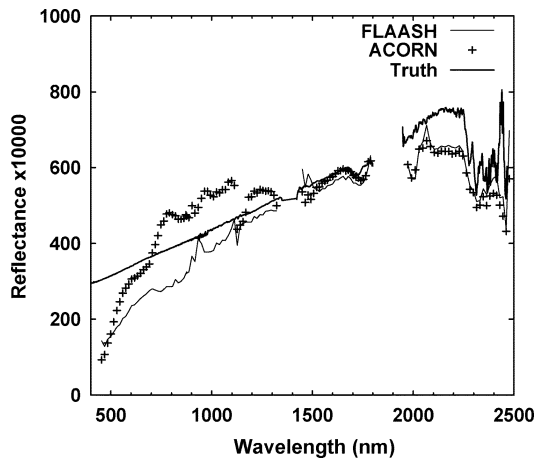

Fig. 5. Default retrievals from FLAASH and ACORN from HyMap image 2 for the large black tarp.

scaling the midlatitude summer model profile to the measured humidity at the ground.

E. FLAASH Reflectance Spectra

The most useful and reliable comparisons between FLAASH-retrieved and ground truth reflectance spectra are for the large black and white tarps in HyMap images 1 and 2. The black tarp retrieval is very sensitive to the modeling of diffuse scattering, while the white tarp retrieval is sensitive to the direct transmittance, hence the visibility.

The FLAASH results for the large black tarp show a systematic trend of slightly increasing reflectance with increasing solar elevation (decreasing solar zenith angle), indicating a small amount of specularity in the material. Since the ground truth measurement was made closest to the time of the HyMap image 2, we compare the ground truth spectrum with the result from that image. The ground truth measurement for the large white tarp was made close to the time of image 1. Aside from the saturation effect mentioned earlier, the FLAASH results for the large white tarp were virtually identical for images 1 and 2, indicating that the tarp behaved as a Lambertian reflector.

Representative HyMap reflectance spectra from FLAASH are shown in Figs. 2 and 3. These were calculated assuming a lower-limit estimate of 50-km visibility, $\Delta N = 0.4$, ozone SF $= 1.24$, and CSF values of 1.0 and 3.5. The effect of the ozone SF is minimal. The retrieved and ground truth reflectances are all in excellent agreement. RMS reflectance errors computed for the overlapping spectral ranges are 0.023 (CSF $= 1.0$) and 0.020 (CSF $= 3.5$) for the white tarp and 0.0054 (CSF $= 1.0$) and 0.0068 (CSF $= 3.5$) for the black tarp. For both tarps the CSF $= 3.5$ (SSA ~ 0.85) curves provide slightly better overall agreement below $\sim$700 nm, while above this wavelength the CSF $= 1$ (SSA ~ 0.96) curves provide slightly better agreement. This is qualitatively consistent with the MFRSR-inferred wavelength dependence of the SSA.

Figs. 4 and 5 show the results of processing image 2 using the FLAASH default settings, with no inputs from the radiometers—that is, using default atmospheric parameters (rural aerosol, $\Delta N = 0$, ozone SF $= 1$, CSF $= 1$) and the land method for visibility retrieval. The retrieved visibility was 30 km. Because this is an underestimate, the reflectance results are slightly less accurate than those in Figs. 2 and 3 (RMS errors are 0.031 for the white tarp and 0.0079 for the black tarp).

F. ACORN Reflectance Spectra

Figs. 4 and 5 show the ACORN results obtained by Hyvista. Since the ACORN-inferred visibilities, and hence transmittances, are too high, the white tarp spectra are significantly underpredicted (the RMS reflectance error is 0.10). The black panel RMS error, 0.0082, is very similar to that from FLAASH with its default settings; however, the spectral shape is less accurate. In particular, there is a jump of around 0.01 at $\sim$700 nm, which may be due to an uncorrected adjacency effect involving the scene vegetation. In addition, there is a negative error below $\sim$550 nm, similar to what is seen in other ACORN spectra [14], which may be systematic. It should be noted that the ACORN results were obtained using the original supplied wavelengths, which are not as precise as the recalibrated values from FLAASH, resulting in peaks or valleys at the edges of atmospheric absorption bands (e.g., at $\sim$1100 nm).

V. Summary and Conclusion

The current analysis of UV and VIS shadowband radiometer (MFRSR) data with simultaneous hyperspectral and multispectral imagery and *in situ* reflectance measurements provides both algorithm validation and insight on first-principles atmospheric compensation. For the clear-weather Davis experiment, there is reasonable self-consistency between aerosol property retrievals inferred from the radiometers and from the imagery, allowing for uncertainty in the vertical distribution of aerosol. Furthermore, there is very good agreement between the FLAASH-corrected reflectance spectra and the ground truth measurements, particularly when the visibility is assumed to be close to that given by the VIS-MFRSR.

The MFRSR results served as a benchmark for the automated visibility retrieval algorithms in FLAASH and ACORN. In addition, it led to a refinement of the two-band water pixel method, adopted as a default in the latest version of ENVI FLAASH, in which the shorter wavelength channel is thresholded for pixel selection. With the Landsat-7 data, the visibilities retrieved by FLAASH using reflectance ratio-based methods with both dark land and water pixels were consistent to within the geographic variability of the aerosol, and in good agreement with the MFRSR measurement. With the HyMap data, acquired from much lower altitudes, the land-pixel method significantly underestimated the visibility, while the water-pixel method gave somewhat closer results. In the latter case, results similar to the water-pixel method would have been obtained from the land-pixel method by using a slightly higher value of the 660–2200-nm reflectance ratio (around 0.50). The visibilities estimated by ACORN from the HyMap imagery were much too high, and agreement of ACORN's reflectance retrievals with the ground truth was not as good as with FLAASH.

The MFRSR data analysis found significant wavelength dependence of the aerosol single-scattering albedo (SSA), ranging from $\sim$0.75 at 368 nm to 0.9–1.0 in the visible. These values are within the range of SSAs measured in clear weather around the world [13], [18], [19], and the visible values are compatible with the commonly used rural aerosol model. The increase in SSA with increasing wavelength is qualitatively supported by the HyMap imagery analysis, and could be explained by a mineral dust or organic aerosol component, which is not contained in the rural model. In general, SSAs are often wavelength dependent [13]–[19], making it problematic to use a UV-derived value for atmospheric compensation of VIS-SWIR-NIR imagery.

With imagery taken in clear weather and containing water bodies or other dark surfaces that enable good scene-based visibility retrieval, the value-added from radiometer-derived atmospheric quantities is modest, partly because there is little aerosol compensation needed in this case. Radiometer-retrieved AODs, SSAs, and column water amounts are sensitive to calibration errors, and the actual AOD can vary geographically. On the other hand, diffuse fluxes directly correlate with the atmospheric backscatter, so that for dark surfaces, which are backscatter-sensitive, there is considerable cancellation of calibration-related SSA and AOD errors in the atmospheric compensation. It should be cautioned that diffuse fluxes are useful for SSA determination only under cloud-free conditions. With imagery acquired during heavy aerosol loading, scattering effects (including the adjacency effect [6]) are much more pronounced. Here, radiometer data should prove highly valuable for atmospheric compensation. It would be very useful to demonstrate this with additional field experiments.

As illustrated here, an application that benefits from a radiometer-derived AOD, even under clear conditions, is the retrieval of reflectance spectra of bright materials, which are especially sensitive to the atmospheric transmittance. It is very difficult to retrieve an accurate total vertical AOD from remote imagery with a dark pixel method when the sensor is only a few kilometers above the ground, because the result is sensitive to the assumed altitude profile of the aerosol, and hence the boundary layer thickness and upper atmospheric aerosol content.

Acknowledgment

The authors are grateful to a number of individuals whose efforts were critical to the success of this project: A. Zachor for assistance with algorithm development, C. Kennedy (ITT), N. Kendall (UC Davis), and M. Mata (UC Davis) for field experiment planning and logistical assistance, G. Scott (Colorado State University) for providing the analyzed UV-MFRSR data, G. Anderson (Air Force Research Laboratory) for technical discussions, and B. Spiering, our contract monitor at the NASA Stennis Space Center.

References

[1] L. Harrison, J. Michalsky, and J. Berndt, "Automated multifilter rotating shadow-band radiometer: An instrument for optical depth and radiation measurements," *Appl. Opt.*, vol. 33, pp. 5118–5125, 1994.

[2] R. Schoemaker and G. deLeeuw, "ATSR-2 retrievals of AOD: Some recent results for year 2000 data over Europe," in *Eos Trans. AGU*, vol. 85, 2004.

[3] P. J. Ricchiazzi and C. Gautier, "Sensitivity of clear-sky diffuse radiation to *in situ* aerosol scattering parameters," presented at the *13th ARM Science Team Meeting Proceedings*, Broomfield, CO, Mar. 31–Apr. 4 2003.

[4] R. N. Halthore and S. E. Schwartz, "Comparison of model-estimated and measured diffuse downward irradiance at surface in cloud-free skies," *J. Geophys. Res.*, vol. 105, pp. 20 165–21 077, 2000.

[5] M. W. Matthew, S. M. Adler-Golden, A. Berk, S. C. Richtsmeier, R. Y. Levine, L. S. Bernstein, P. K. Acharya, G. P. Anderson, G. W. Felde, M. P. Hoke, A. Ratkowski, H.-H. Burke, R. D. Kaiser, and D. P. Miller, "Status of atmospheric correction using a MODTRAN4-based algorithm," in *Proc. SPIE Conf. Algorithms for Multispectral, Hyperspectral, and Ultraspectral Imagery VI*, vol. 4049, 2000, pp. 199–207.

[6] M. W. Matthew, S. M. Adler-Golden, A. Berk, G. Felde, G. P. Anderson, D. Gorodetzky, S. Paswaters, and M. Shippert, "Atmospheric correction of spectral imagery: Evaluation of the FLAASH algorithm with AVIRIS data," in *Proc. SPIE Conf. Algorithms and Technologies for Multispectral, Hyperspectral, and Ultraspectral Imagery IX*, 2003.
[7] *ACORN 4.0 User's Guide*, ImSpec LLC, Palmdale, CA, 2002.
[8] A. Berk, G. P. Anderson, P. K. Acharya, M. L. Hoke, J. H. Chetwynd, L. S. Bernstein, E. P. Shettle, M. W. Matthew, and S. M. Adler-Golden, *MODTRAN4 Version 3 Revision 1 User's Manual*. Hanscom AFB, MA: Air Force Res. Lab./Space Vehicles Directorate, 2003, vol. 91.
[9] M. B. Satterwhite and C. S. Allen, "A novel, low cost approach for large gray-toned fabric panels for calibrating remotely sensed VIS/NIR/SWIR data," presented at the *AeroSense, Technologies and Systems for Defense and Security, International Society for Optical Engineering*, Apr. 21–25, 2003, 5093-19.
[10] R. L. Kurucz, "The solar irradiance by computation," in *Proc. 17th Annu. Review Conf. Atmospheric Transmission Models*, G. P. Anderson, R. H. Picard, and J. H. Chetwynd, Eds., May 1995. PL/-TR-95-2060, Special Reports, no. 274, Pl. 332, Phillips Laboratory/Geophysics Directorate, MA.
[11] J. J. Michalsky, J. C. Liljegren, and L. C. Harrison, "A comparison of sun photometer derivations for total column water vapor and ozone to standard measures of same at the Southern Great Plains atmospheric radiation measurement site," *J. Geophys. Res.*, vol. 100, pp. 25 995–26 003, 1995.
[12] S. M. Adler-Golden, P. K. Acharya, A. Berk, M. W. Matthew, and D. Gorodetzky, "Remote bathymetry of the littoral zone from AVIRIS, LASH, and QuickBird imagery," *IEEE Trans. Geosci. Remote Sens.*, vol. 43, no. 2, pp. 337–347, Feb. 2005.
[13] J. L. Petters, V. K. Saxena, J. R. Slusser, B. N. Wenny, and S. Madronich, "Aerosol single scattering albedo retrieved from measurements of surface UV irradiance and a radiative transfer model," *J. Geophys. Res.*, vol. 108, no. D9, p. 4288, 2003.
[14] A. F. Kruse, "Comparison of ATREM, ACORN, and FLAASH atmospheric corrections using low-altitude AVIRIS data of boulder, Colorado," presented at the *13th JPL Airborne Geoscience Workshop*, Pasadena, CA, Mar. 31–Apr. 2 2004.
[15] Y. J. Kaufman, D. Tanre, L. A. Remer, E. F. Vermote, A. Chu, and B. N. Holben, "Operational remote sensing of tropospheric aerosol over land from EOS Moderate Resolution Imaging Spectroradiometer," *J. Geophys. Res.*, vol. 102, pp. 17 051–17 067, 1997.
[16] R. G. Isaacs, W. C. Wang, R. D. Worsham, and S. Goldenberg, "Multiple scattering LOWTRAN and FASCODE models," *Appl. Opt.*, vol. 26, pp. 1272–1281, 1987.
[17] K. Stamnes, S.-C. Tsay, W. Wiscombe, and K. Jayaweera, "Numerically stable algorithm for discrete-ordinate-method radiative transfer in multiple scattering and emitting layered media," *Appl. Opt.*, vol. 27, pp. 2502–2509, 1988.
[18] T. L. Anderson, D. S. Covert, J. D. Wheeler, J. M. Harris, K. D. Perry, B. E. Trost, D. J. Jaffe, and J. A. Ogren, "Aerosol backscatter fraction and single scattering albedo: Measured values and uncertainties at a coastal station in the Pacific northwest," *J. Geophys. Res.*, vol. 104, pp. 26 793–26 807, 1999.
[19] O. Dubovik, B. N. Holben, T. F. Eck, A. Smirnov, Y. J. Kaufman, M. D. King, D Tanré, and I. Slutsker, "Variability of absorption and optical properties of key aerosol types observed in worldwide locations," *J. Atmos. Sci.*, vol. 59, pp. 590–608, 2002.

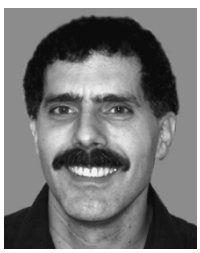

Peter A. Rochford received the B.S. degree in physics from the University of Ottawa, Ottawa, ON, Canada, in 1983 and the Ph.D. degree in theoretical nuclear physics from the University of Toronto, Toronto, ON, in 1989

He is a Principal Scientist at Spectral Sciences, Inc. (SSI), Burlington, MA. Prior to joining SSI in 2002, he was active in ocean modeling and prediction at the Naval Research Laboratory, Stennis Space Center, MS. This research included numerical modeling of upper-ocean processes, air–sea interactions, turbulent mixed-layer dynamics, and ocean biology in global and regional ocean circulation models. His work in numerical modeling included tropical cyclones, atmospheric acoustics, seismology, and nuclear physics. His current interests include high-performance computing, atmospheric and oceanic modeling, and air–sea interactions.

Prabhat K. Acharya received the M.S. degree in computer science from the University of Utah, Salt Lake City, and the Ph.D. degree in chemical physics from the University of North Carolina, Chapel Hill, in 1982 and 1987, respectively. His M.S. work in computer science under the supervision of Profs. Thomas C. Henderson and Bir Bhanu involved applications and development of Hough transform and least squares techniques for range data analysis for computer vision applications. His Ph.D. work in chemistry under the supervision of Prof. Robert G. Parr was in the area of electron density functional theory.

He is currently a Principal Scientist with Spectral Sciences, Inc. (SSI), Burlington, MA. He has extensive experience in the areas of atmospheric radiance and transmission modeling and simulation. He has played a key technical role in the collaborative development by SSI and the Air Force Research Laboratory of the MODTRAN radiation transport code. He is currently engaged in developing very rapid techniques for modeling atmospheric radiance in broad bandpasses. Prior to joining SSI, he was a Postdoctoral Fellow with Prof. Jack Simons at the University of Utah, where he calculated rates and formulated propensity rules for electron autodetachment of vibrationally excited molecules.

Steven M. Adler-Golden received the Ph.D. degree in physical chemistry from Cornell University, Ithaca, NY, in 1979. His Ph.D. work under Prof. John Wiesenfeld was in the area of small molecule photochemistry and spectroscopy.

He is currently the Leader of the Remote Sensing Group at Spectral Sciences, Inc., Burlington, MA. His experience at both the technical and management levels includes atmospheric aeronomy, infrared/visible/ultraviolet radiation modeling, and prototype trace gas sensor development. He has been active in the development of atmospheric compensation and data analysis algorithms for spectral imagery, including the FLAASH algorithm. Prior to joining Spectral Sciences in 1981, he did postdoctoral work on energy transfer in ozone under Prof. Jeffrey Steinfeld at the Massachusetts Institute of Technology.

Alexander Berk received the B.S. degrees in chemistry and mathematics from Harvey Mudd College, Claremont, CA, and the Ph.D. degree from the University of North Carolina, Chapel Hill, in 1978 and 1983, respectively. His Ph.D. research with Professor Robert G. Parr centered on the development and application of techniques for calculation of energy lower bounds, including new expressions for the energy of Hartree–Fock and density functional systems.

He is currently a Principal Scientist and Special Project Director with Spectral Sciences, Inc. (SSI), Burlington, MA. His research activities have concentrated on the modeling of atmospheric absorption, scattering, radiance, flux, and remote sensing phenomena in the infrared, visible, and ultraviolet spectral regions. He has been the lead model developer for the Air Force Research Laboratory radiation transport codes MODTRAN and SAMM. Prior to joining SSI, he held the position of Mathematical Chemist for Sachs/Freeman Associates, Inc. and served as a Postdoctoral Fellow collaborating with Professor Jiri Cizek.

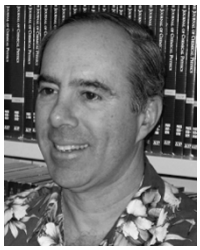

Lawrence S. Bernstein received the Ph.D. degree in physical chemistry from the University of California, Berkeley, in 1974.

This was followed by postdoctoral fellowships at Bell Laboratories and Harvard University involving the spectroscopy of Van der Waals molecules. From 1976 to 1981, he was employed as a Research Scientist at Aerodyne Research, Inc., working in the areas of atmospheric radiative transfer and high-temperature molecular spectroscopy. In 1981, he co-founded Spectral Sciences, Inc., Burlington, MA, where he currently serves as the Chief Scientist.

Michael W. Matthew received the Ph.D. degree in applied mechanics from Yale University, New Haven, CT, in 1982, working under Dr. Peter Wegener in the area of homogeneous nucleation.

He is currently a Principal Scientist with Spectral Sciences, Inc. (SSI), Burlington, MA. He leads the technical development of the FLAASH atmospheric correction code for hyperspectral and multispectral imagery. He has also been active in the continued development of the SSI/Air Force Research Laboratory radiation transport model MODTRAN as well as the development of techniques for chemical species detection and measurement. He did postdoctoral work on ion impact effects under Dr. Lewis Friedman at Brookhaven National Laboratory before joining SSI in 1985.

Steven C. Richtsmeier received the B.S. degree in chemistry from Gustavus Adolphus College, St. Peter, MN, and the Ph.D. degree in physical chemistry from the University of Minnesota, Minneapolis, in 1977 and 1983, respectively. His Ph.D. work under Dr. David A. Dixon was in the field of molecular beam studies.

He is a Principal Scientist at Spectral Sciences, Inc., Burlington, MA, and is currently the technical leader for development of MCScene, a first-principles Monte Carlo hyperspectral imagery simulation code. Other research activities have included development of instrumentation for measurement of trace pollutant gases, and modeling and analysis of infrared, visible, and ultraviolet signatures of aircraft and rockets. Prior to joining Spectral Sciences in 1985, he did postdoctoral work under Dr. Stephen J. Riley at Argonne National Laboratory studying gas phase metal clusters.

Stephen Gulick, Jr., photograph and biography not available at the time of publication.

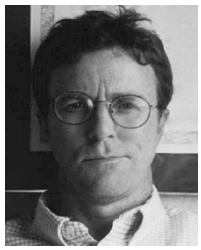

James Slusser received the B.S. and M.S. degrees in physics from Western Michigan University, Kalamazoo, and the Ph.D. degree from the University of Alaska, Fairbanks in 1974 and 1994, respectively. His Ph.D. work was in radiative transfer and trace gas spectroscopy of nitrogen dioxide.

Since 1999, he has served as the Director of the U.S. Department of Agriculture's UV-B Monitoring Program at Colorado State University (CSU). His research interests include aerosol optical properties, atmospheric compensation for satellite imagery, response of plants to increased UV and other climate stressors, and remote sensing of plant stress. He held a postdoctoral position at the Cambridge Chemical Laboratory studying the influence of volcanic aerosols on Antarctic ozone abundances prior to joining CSU in 1996. He has authored or coauthored more than 35 peer-reviewed papers. He was coeditor of four proceedings, two special sections in *Optical Engineering*, and one in *Forest and Agricultural Meteorology*.

Dr. Slusser is active in SPIE, AGU, and AMS and has co-chaired seven national and international meetings.